

Measurement of martensitic packet size by EBSD in the high strength steel X38CrMoV5-1 and estimation of its influence on cleavage fracture

A. Pastor^{1*}, P. Valles¹, P. Pérez², S. F. Medina²

¹Laboratory of Microscopy, National Institute of Aerospace Technology (INTA),
Ctra. Torrejón-Ajalvir km 4, 28850-Torrejón de Ardoz, Spain

²Department of Physical Metallurgy, National Centre for Metallurgical Research (CENIM-CSIC),
Av. Gregorio del Amo 8, 28040-Madrid, Spain

Received 21 October 2019, received in revised form 14 May 2020, accepted 14 May 2020

Abstract

The crystallographic packet or microstructural unit was determined with 15° and 5° boundary grain misorientations in a quenched and tempered X38CrMoV5-1 steel, yielding results of 0.68 and 0.59 μm, respectively. Though both values are similar, the latter has been taken as the best to calculate the effective surface energy of cleavage fracture, γ_p , leading to a value of 15.8 J m⁻². Thus it is demonstrated that the microstructural unit controlling crack propagation is that determined by EBSD with a 5° misorientation angle. Other structural parameters, like the parent austenite grain size and the morphological martensitic packet, have been ruled out.

Key words: EBSD, crack growth, fracture toughness, precipitation, steel

1. Introduction

X38CrMoV5-1 (H11) steel is widely employed in hot forming applications such as pressure die casting for light alloy injection. Its martensitic microstructure presents a hardness ranging between 40 and 56 HRC depending on the tempering temperature, which is usually between 550 and 600 °C. Its most common application is as hot work tool steel, but its high strength makes it suitable for manufacturing safety parts that require high strength (1400 MPa) and a minimum absorbed energy of 12 J [1].

In martensitic and also in bainitic transformations, each parent austenite grain is transformed into one or more martensitic packets, depending on the grain size [2]. Martensitic nucleation is heterogeneous and takes place at the austenite grain boundaries and defects such as dislocations. The transformation ends when the laths or plates reach the parent austenite grain boundaries. Each packet is characterized by the formation of thin parallel laths constituting a homogeneous group. The parent austenite phase and marten-

site constituent show a Kurdjumov-Sachs relationship [3, 4].

Each packet is further divided into parallel blocks, each of which contains a group of laths with the same or similar orientation. Since both the packet and block boundaries are high angle boundaries, the two constituents are considered to be effective grains and to strongly affect the strength and toughness of steels [5–8]. The martensitic packet size has also been related to the unit crack path (UCP) [6], while other authors consider the block size to be more relevant in brittle fractures and crack propagation [8–10].

Some authors have confirmed that the microstructural unit controlling cleavage crack propagation is the crystallographic packet defined by electron backscattered diffraction (EBSD) because crystallographic packet limits with a certain misorientation angle are able to stop microcrack propagation [11, 12] effectively. Others have reported that a 10°–15° misorientation between cleavage planes {100} corresponding to two adjacent crystallographic packets could no-

*Corresponding author: tel.: +00-34-915206369; e-mail address: pastorma@inta.es

Table 1. Chemical composition (wt.%) of the steel used

Fe	C	Si	Mn	Cr	Mo	V	Al	P	S	N
Base	0.35	1.07	0.40	5.2	1.2	0.42	0.03	< 0.01	0.011	0.0248

tably modify crack propagation in a brittle fracture [13].

Cleavage fracture crack propagation in high strength martensitic alloys has not hitherto been widely studied. This paper seeks to analyze the brittle fracture of these steels using EBSD to determine the size of a martensitic crystallographic packet with 15° and 5° misorientations in a hot rolled quenched and tempered X38CrMoV5-1 steel. The influence of this microstructural parameter on cleavage fracture is also examined concerning Griffith's theory.

In recent work, it has been shown that lost wax casting, also known as investment casting or precision casting, is not an appropriate method for the manufacturing of elevator safety system parts. Parts manufactured by lost wax casting present micropores with an approximately elliptic shape can cause a catastrophic fracture in service by cleavage at stresses well below the yield strength. Most of these parts do not pass impact tests with 50 kN loads [14], whereas parts manufactured by machining and with the same quenching and tempering heat treatment pass all impact tests.

It was also established that the tensile mechanical properties obtained, especially ductility and Charpy impact toughness, are better than those achieved by casting [15]. This work thus demonstrates that the absence of micropores in the machined parts is what allows them to pass the impact test with a load of 50 kN, and that crack propagation is controlled by the nanometric crystallographic unit.

2. Materials and methods

In previous studies, the authors have shown that parts manufactured by wax casting can be used as safety components in equipment such as lifts, despite the fact that dendritic microporosity can cause brittle fracture at loads well below the yield strength [1]. In the present work, a X38CrMoV5-1 steel has been manufactured by continuous casting and hot rolling to obtain a 25 mm thickness porosity-free plate. The chemical composition of this steel is given in Table 1.

As a result of a previous study involving the use of dilatometry, it is possible to obtain the continuous cooling transformation diagram and to determine the tempering treatments needed to optimize the heat treatment [16]. The optimal heat treatment consists of annealing at 780°C for 1 h and cooling in the furnace, followed by quenching treatment from 1020°C for 1 h,

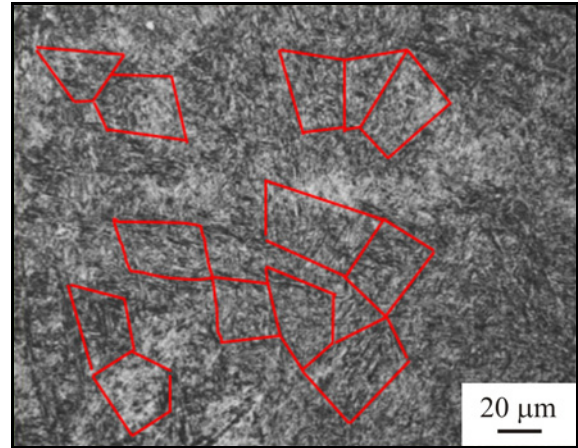


Fig. 1. Martensite microstructure. Some martensitic packets have been framed.

cooling in oil, and double tempering at 580°C for 2 h.

Microtexture analysis of this steel was carried out by EBSD attached to SEM equipment (field emission JEOL JSM 6500F). EBSD data was analyzed using Channel 5 EBSD software. For orientation image mapping, the scan step was set at $0.08\text{--}0.1\ \mu\text{m}$ and the area inspected was $25.5\ \mu\text{m} \times 20\ \mu\text{m} = 510\ \mu\text{m}^2$.

Tensile tests were performed with a 100 kN MTS servohydraulic unit according to standard ASTM E8-04 with specimen dimensions of 6.3 mm diameter and 25 mm gauge length. Charpy test specimens were $10 \times 10 \times 55\ \text{mm}^3$ in size with a V-shaped notch 2 mm deep and a notch opening of 45° , following standard ASTM E-23. All the tests were carried out at room temperature.

3. Results and discussion

3.1. Microstructure analysis

The microstructure obtained is tempered martensite constituted mainly by small laths grouped in packets and some plates (Fig. 1). The parent austenite shows an average grain size of approximately $80\ \mu\text{m}$ measured according to standard ASTM E-112. The average martensitic packet size is shown delimited by red lines in Fig. 1. The packet size is given by $l = \sqrt{l_1 l_2}$, where l_1 and l_2 are the average packet length and width, respectively.

The average value of l was calculated by observing

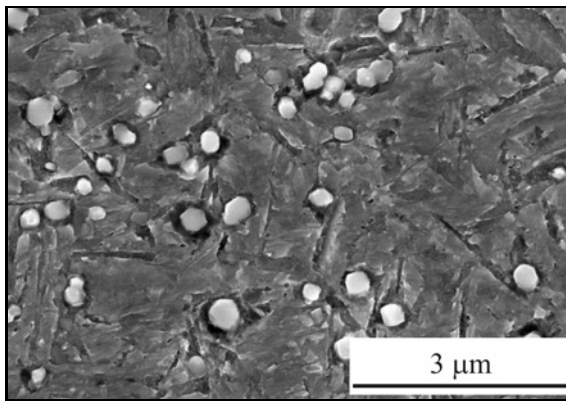


Fig. 2. SEM image showing VCN precipitates.

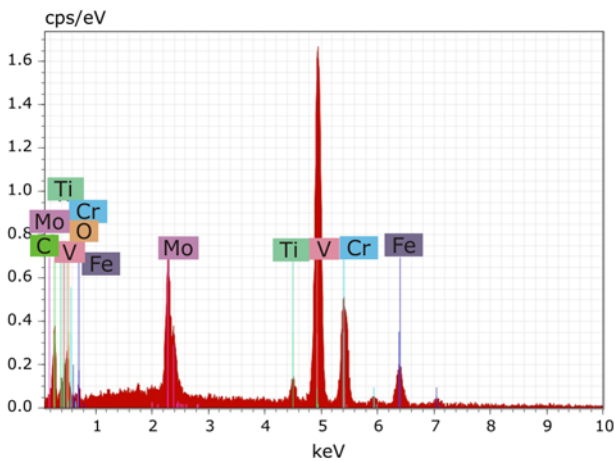


Fig. 3. Energy-dispersive X-ray spectrum of a VCN precipitate.

50 packets by optical microscopy, yielding a result of $29 \mu\text{m}$. The criteria followed to delimit a martensitic packet is the parallelism or alignment of the martensite laths. In this case, the definition of a morphological packet as defined by optical microscopy is used instead of the definition of a crystallographic packet as mentioned above.

A secondary phase of vanadium carbonitrides (VCN) was observed by electron scanning microscopy, as shown in Fig. 2. These precipitates, which are spherical, are relatively abundant as a consequence of the high percentages of vanadium and nitrogen present in the steel.

The EDX spectrum of a precipitate is shown in Fig. 3. The interaction volume of EDX analysis is larger than the precipitate itself. So the EDX spectrum shows elements belonging to the chemical composition of the matrix as well as those corresponding to the precipitate.

The precipitate size was measured over a population of approximately 150 particles, and the results are

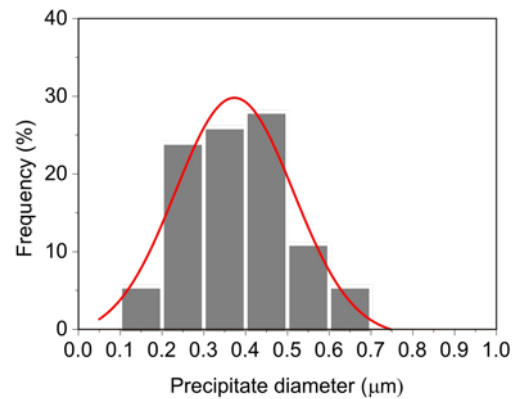


Fig. 4. Frequency distribution of precipitate sizes (diameter). Measured error < 3%.

shown in the histogram in Fig. 4, where their diameter ranges are between 0.1 and $0.7 \mu\text{m}$. This distribution is normal or Gaussian, and the Gaussian function is overdrawn. According to the Gaussian function, the weighted average diameter measured was $0.37 \mu\text{m}$. The precipitate size is half the sum of two perpendicular diameters that were measured by zooming the PC screen image 5 times in each micrograph. The error is twice the unit of measurement (0.5 mm), which considering the scale and the screen zoom would be less than 3%.

3.2. Electron backscattered diffraction (EBSD) analysis

In the EBSD technique, the distinction of grains is based on the study of crystallographic orientations. This allows the microstructural units to be distinguished according to their misorientation through a selected grain boundary, considering two adjacent grains as different units [2].

EBSD analysis was carried out on heat-treated tempered martensite specimens, as mentioned above. The specimens were polished up to mirror condition with colloidal silica. Two different grain boundary misorientation tolerance criteria, 15° and 5° were considered. Figures 5a,b show the inverse pole figures, denominated as orientation maps for the 15° and Figs. 5c,d for 5° misorientations, respectively, which allow the grain distribution to be studied.

The grain distribution is different when measured by optical microscopy, where each grain distribution is shown directly, or by EBSD, where it is measured by misorientation. The latter technique is used by many authors to calculate the size of the crystallographic martensite packet.

Martensite laths with different orientations can be developed from the original parent austenite grains, especially at grain boundaries. However, some of the

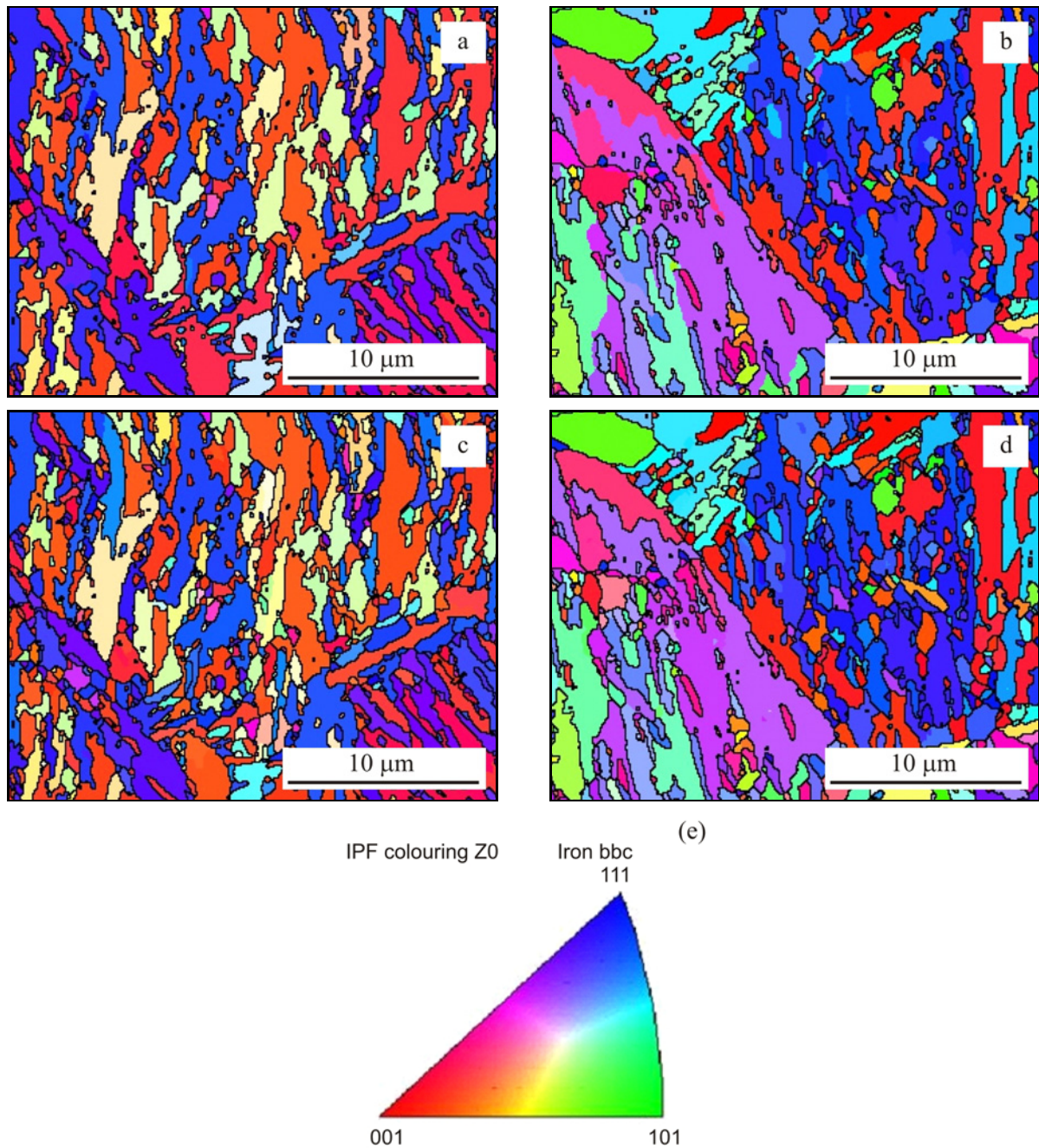


Fig. 5. Inverse pole figures (IPF) maps: (a), (b) misorientation 15° ; (c), (d) misorientation 5° ; (e) key for IPF maps.

laths may correspond to martensite laths coming from other neighbouring grains outcropping in the metallographic section used for EBSD measurements. As this factor cannot be corrected, the average size of martensite laths from EBSD measurements, calculated in Figs. 6 and 7, is underestimated with respect to the true value. As expected, the average size of the martensitic crystallographic unit decreases from 0.68 to $0.59 \mu\text{m}$ when the misorientation criterion for discriminating grain boundaries is varied from 15° to 5° .

Once martensite nucleates it is well known that its length grows at rates near to the speed of sound. Thus

the relationship between the thickness and length of martensite laths remains almost constant [17], and their growth is halted by the plastic deformation produced during the transformation. The calculated values of between 0.59 and $0.68 \mu\text{m}$ for the martensitic crystallographic unit are a little higher than the average width of martensite laths, about $0.30 \mu\text{m}$ measured by optical microscopy. Thus it can be said that the crystallographic martensitic packet size measured by EBSD for a 15° misorientation is almost twice the width of a single martensite lath.

For some authors, martensite laths may cause

Table 2. Mean values of mechanical properties in tensile test and absorbed energy in the Charpy test

Yield strength (MPa)	Ultimate strength (MPa)	Area reduction (%)	Absorbed energy (J)
1273	1506	42	20

Uncertainty of yield strength and ultimate strength = 0.5 %

Uncertainty of absorbed energy < 3 J

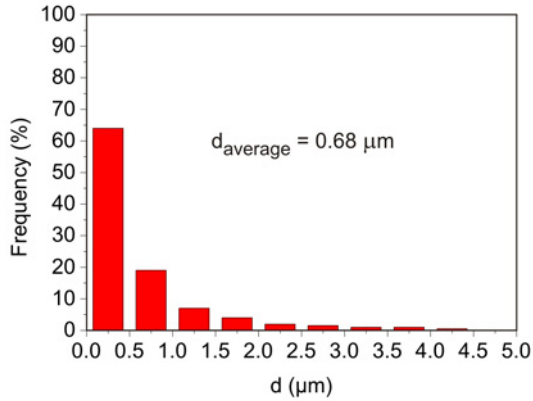


Fig. 6. Frequency of crystallographic unit size at 15° misorientation.

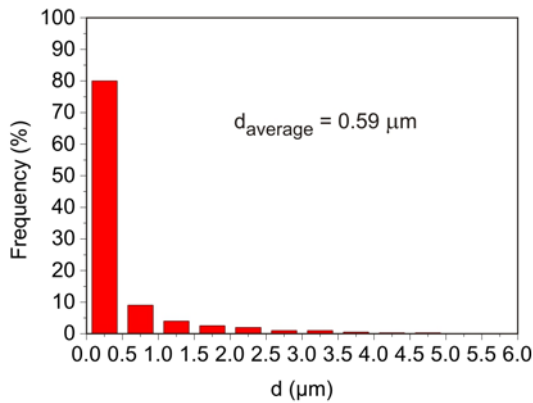


Fig. 7. Frequency of crystallographic unit size at 5° misorientation.

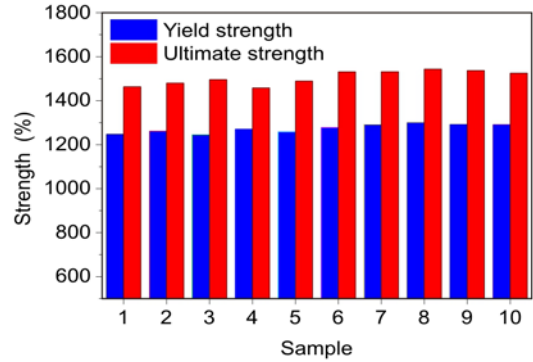


Fig. 8. Yield strength and ultimate strength determined for ten specimens.

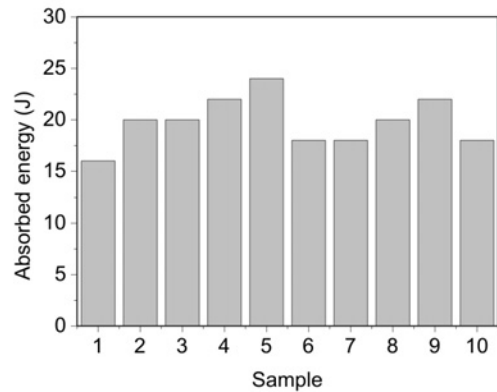


Fig. 9. Absorbed energy in Charpy impact test determined for ten specimens.

a brittle fracture, and in high strength steels like X38CrMoV5-1, the fracture would be produced by cleavage and would be transgranular [5].

3.3. Griffith's equation application to cleavage fracture

X38CrMoV5-1 tool steel has to withstand the highest stresses in hot-forging and die-casting applications, where loading conditions are very complex and vary from point to point on the tool [18].

The mechanical properties of the steel were determined in a tensile test. Ten specimens were prepared with the optimized heat treatment mentioned above

and machined parallel to the rolling direction. Average values for yield strength, ultimate strength, and area reduction are listed in Table 2. These values correspond to the average of ten specimens tested. The 0.5% error is given by the measurement uncertainty based on the calibration results carried out according to the ISO 376 standard.

In addition to this, absorbed energy in the Charpy impact test was determined for another ten specimens and is shown in Table 2. As the steel was hot rolled, all the micropores formed during dendritic solidification disappeared, obtaining a compact material. The yield and ultimate strength values are illustrated in Fig. 8, while the absorbed energy in the Charpy impact test is

plotted in Fig. 9. The uniformity of all the values is a consequence of a uniform martensitic microstructure, free of defects (cracks or pores) that may cause a sharp decrease in mechanical properties.

The values in Table 2 are close to those found in the same steel X38CrMoV5-1 by other authors with the same or similar heat treatment conditions [19]. According to these values, the steel presents high strength and absorbed energy of 20 J, which is optimum for this type of steels. Nevertheless, this continues to be a low value, and the steel may, therefore, present cleavage or brittle fracture due to the low plastic deformation. The uncertainty of the energy absorbed in the Charpy impact test is also given by the calibration results, being < 3 J.

The general form of Griffith's equation is [20]:

$$\sigma_f = \left(\frac{4E\gamma_p}{\pi(1-\nu^2)d} \right)^{\frac{1}{2}}, \quad (1)$$

where σ_f is the microscopic (local) cleavage fracture stress at the tip of the microcrack, E is Young's modulus, ν is Poisson's ratio ($\nu = 0.3$), γ_p is the effective surface energy of cleavage fracture, and d is equal to the critical microcrack length for cleavage fracture.

The importance of Eq. (1) is basically due to the relationship established between σ_f and the square root of the crack size. Other authors have also used Eq. (1) to seek a connection between the microstructural unit and "d". For martensite laths, where a high dislocation density may cause a brittle fracture without any plastic deformation, some researchers accept a γ_p value of between 7–9 J m⁻² [21, 22] while others increase this value up to 14 J m⁻² [23]. On the other hand, it has also been suggested that the cleavage fracture stress σ_f could be used as an engineering notch toughness parameter for specific materials to assess the integrity of structures with notch defects [24].

The critical cleavage stress σ_f has been calculated using the Tresca criterion for a Charpy-V specimen [25, 26], giving:

$$\sigma_f = 2.18\sigma_y, \quad (2)$$

where σ_y is the uniaxial yield stress obtained in a tensile test corresponding to 0.2% proof stress ($\sigma_{0.2}$).

Inserting in Eq. (2) the yield strength from Table 2 ($\sigma_y = \sigma_{0.2} = 1273$ MPa), the value for σ_f is 2775 MPa, which is relatively high and corresponds to a very small microstructural unit or defect. This σ_f value is in accordance with the values calculated by other authors for low C steels with a martensitic microstructure [21, 22, 26]. Finally, considering Eq. (1), γ_p values are calculated for each different microstructural unit measured: the austenite grain size (because grain boundaries remain after the martensitic transformation), the morphological size of the martensitic

Table 3. Values of the effective surface energy of cleavage fracture (γ_p) for several microstructural units

Microstructural unit	The energy of cleavage fracture γ_p (J m ⁻²)
Austenite grain size (80 μm)	2267
Martensite packet (29 μm)	822
Misorientation 15° (0.68 μm)	18.2
Misorientation 5° (0.59 μm)	15.8

packet, and the crystallographic unit size determined for 15° and 5° misorientations, respectively (Table 3).

For the calculation, Young's modulus value of 205 GPa was used, which corresponds to the average value for quenched and tempered hypoeutectoid steels with a similar C content [27]. Thus, the effective surface energy of cleavage fracture (γ_p) results, presented in Table 3, show that the austenite grain and the morphological martensitic packet cannot be the microstructural unit controlling the cleavage fracture in quenched steels with a lath martensite microstructure.

Moreover, the unit crack path (UCP) is defined as the region where the crack propagates as a straight line [26]. The relationship between the UCP and the microstructural unit (mu) where the crack is generated, presenting approximately the same size as the unit and followed by its unit to unit propagation, has been studied by several authors. Values for $\langle \text{UCP} \rangle / d_{\text{mu}}$ relationships, where d_{mu} was measured by EBSD, vary from 1.2 for an upper bainite packet [25] followed by an intermediate value of 1.3 for a polygonal ferrite packet [28, 29] and 1.5 for a lower bainite packet [30]. In the medium or high C steels, lower bainite presents a similar toughness to that observed in martensitic tempered steels. Therefore it seems logical to use the 1.5 relationship for this studied steel. So, the UCP for a 5° misorientation would be in the maximum range of 0.88 μm .

Comparison of the results obtained in this study with others obtained for bainitic microstructures [2] shows that in the latter case the unit calculated by EBSD with a 15° misorientation is the microstructural characteristic controlling the crack propagation, causing a brittle fracture. However, in the present case, the microstructural unit calculated with a 5° misorientation is close to the microcrack length, which will cause a cleavage fracture, as the value calculated for effective surface energy is 15.8 J m⁻², very close to the above mentioned 14 J m⁻².

It is interesting to note that in bainitic steels with an upper bainitic microstructure, the microstructural characteristic or unit responsible for crack formation and its propagation presents larger dimensions that in

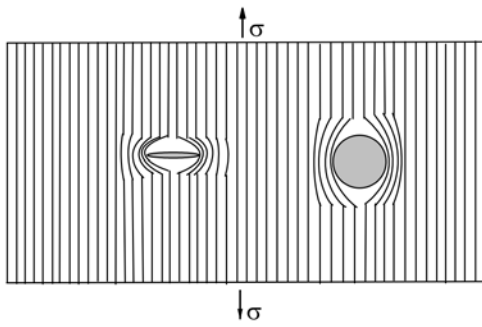


Fig. 10. Scheme of stress intensity at a microcrack tip and a spherical precipitate.

this studied case, which justifies a higher toughness in martensitic steels than in bainitic steels with similar ultimate strength. Equation (1) has been used in this study to determine the critical microcrack length that propagates when subjected to loads, irrespective of where the crack origin is located.

In this tempered martensitic microstructural steel with approximately spherical VCN precipitates, Curry and Knot [22] consider that crack nucleation will be originated in the breakage of some precipitate, particularly the larger ones. Its propagation will be through the matrix because the presence of precipitates is not significant enough for the distance between them to be equal to or less than the calculated microstructural unit. Although the spherical shape of the precipitates is different from the elliptic crack that nucleates in a cleavage fracture, the simple scheme shown in Fig. 10 shows that although the local load increases at the martensite/particle interface surface, it is less than that found at the microcrack tip.

Figures 11a,b show several fractographs of the fracture surface at different magnifications from the Charpy test specimens. These images reveal a cleavage fracture where no voids can be seen, and this is an indication that there was no plastic deformation. In Fig. 11a some river marking is observed, a typical sign of cleavage fracture.

Finally, it can be said that the reason that the machined parts have passed the elevator manufacturer's impact test with loads of up to 50 kN [14] is due to the absence of micropores which were present in the parts manufactured by lost wax casting.

4. Conclusions

Crack nucleation should originate in the breakage of VCN precipitates, especially the larger ones. The martensitic crystallographic unit size determined by EBSD with a 5° misorientation controls crack propagation in cleavage fracture. The microstructural unit

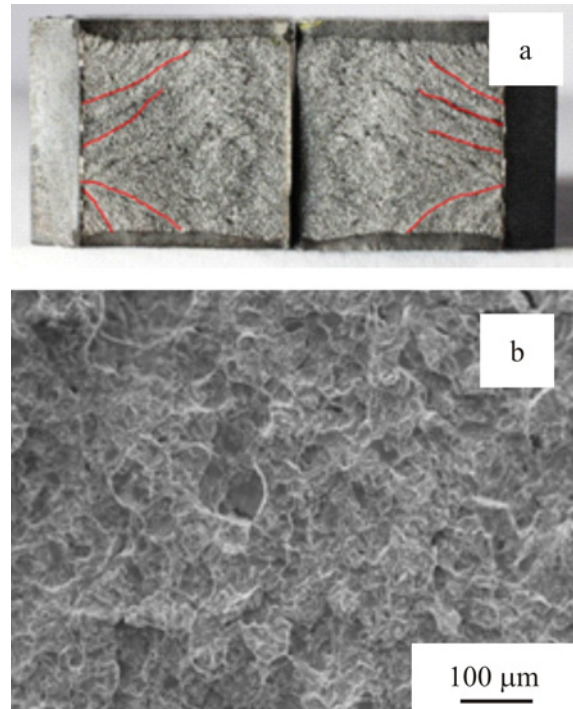


Fig. 11. Fracture surface of Charpy-V-notch specimen of steel tested at 22 °C: (a) fractograph and (b) SEM image.

or characteristic size is 0.59 μm, giving an average UCP size of approximately 0.88 μm. Inserting this value of 0.59 μm in Griffith's equation leads to an effective surface energy (γ_p) value of 15.8 J m⁻², very similar to the values given by other authors. The other microstructural parameters, like the parent austenite grain size and the morphological martensitic packet, yield such high γ_p values that they can be ruled out as being responsible for crack formation and propagation.

Acknowledgement

We acknowledge the financial support of the Spanish CICYT (Project MAT 2011-29039-C02-02).

References

- [1] A. Pastor, P. Valles, I. Amurrio, S. F. Medina, Heat treatment conditions to prevent failure in die cast X38CrMoV5 steel parts, *Eng. Fail. Anal.* 56 (2015) 520–529. [doi:10.1016/j.engfailanal.2014.11.016](https://doi.org/10.1016/j.engfailanal.2014.11.016)
- [2] L. Rancel, M. Gómez, S. F. Medina, I. Gutierrez, Measurement of bainite packet size and its influence on cleavage fracture in a medium carbon bainitic steel, *Mater. Sci. Eng. A* 530 (2011) 21–27. [doi:10.1016/j.msea.2011.09.001](https://doi.org/10.1016/j.msea.2011.09.001)
- [3] C. C. Kinney, I. Yi, K. R. Pytlewski, A. G. Khachatryan, N. J. Kim, J. W. Morris, The microstructure of

- as-quenched 12Mn steel, *Acta Mater.* 25 (2017) 442–454. [doi:10.1016/j.actamat.2016.12.001](https://doi.org/10.1016/j.actamat.2016.12.001)
- [4] V. M. Gundyrev, V. I. Zeldovich, V. M. Schastlivtsev, Crystallographic analysis of the martensitic transformation in medium-carbon steel with packet martensite, *Phys. Met. Metallogr.* 117 (2017) 1017–1027. [doi:10.1134/S0031918X16100100](https://doi.org/10.1134/S0031918X16100100)
- [5] C. Wang, H. Qiu, Y. Kimura, T. Inoue, Morphology, crystallography, and crack paths of tempered lath martensite in a medium-carbon low-alloy steel, *Mater. Sci. Eng. A* 669 (2016) 48–57. [doi:10.1016/j.msea.2016.05.041](https://doi.org/10.1016/j.msea.2016.05.041)
- [6] Y. Tomita, K. Okabayashi, Effect of microstructure on strength and toughness of heat-treated low alloy structural steels, *Metall. Trans. A* 17 (1986) 1203–1209. [doi:10.1007/BF02665319](https://doi.org/10.1007/BF02665319)
- [7] C. F. Wang, M. Q. Wang, J. Shi, W. J. Hui, H. Dong, Effect of microstructure refinement on the strength and toughness of low alloy martensitic steel, *J. Mater. Sci. Technol.* 23 (2007) 659–664.
- [8] A. Shibata, T. Nagoshi, M. Sone, S. Morito, Y. Higo, Evaluation of the block boundary and sub-block boundary strengths of ferrous lath martensite using a micro-bending test, *Mater. Sci. Eng. A* 527 (2010) 7538–7544. [doi:10.1016/j.msea.2010.08.026](https://doi.org/10.1016/j.msea.2010.08.026)
- [9] S. Morito, H. Yoshida, T. Maki, X. Huang, Effect of block size on the strength of lath martensite in low carbon steels, *Mater. Sci. Eng. A* 438–440 (2006) 237–240. [doi:10.1016/j.msea.2005.12.048](https://doi.org/10.1016/j.msea.2005.12.048)
- [10] J. C. Shen, Z. J. Luo, C. F. Yang, Y. Q. Zhang, Effective grain size affecting low temperature toughness in lath structure of HSLA steel, *J. Iron Steel Res.* 26 (2014) 70–76.
- [11] A. F. Gourgues, H. M. Flower, T. C. Lindley, Electron backscattering diffraction study of acicular ferrite, bainite, and martensite steel microstructures, *Mater. Sci. Technol.* 16 (2000) 26–40. [doi:10.1179/026708300773002636](https://doi.org/10.1179/026708300773002636)
- [12] J. Nohava, P. Haušild, M. Karlík, P. Bompard, Electron backscattering diffraction analysis of secondary cleavage cracks in a reactor pressure vessel steel, *Mater. Charact.* 49 (2002) 211–217. [doi:10.1016/S1044-5803\(02\)00360-1](https://doi.org/10.1016/S1044-5803(02)00360-1)
- [13] E. Mazancová, Z. Jonsta, P. Wyslych, K. Mazanec, Acicular ferrite and bainite microstructure properties and comparison of their physical metallurgy response, *Proceedings of 14th International Metallurgical and Materials Conference (Metal 2005)*, paper no. 26. ISBN 80-806840-13-1
- [14] A. Pastor, P. Valles, J. A. Jiménez, S. F. Medina, Microstructural analysis of X38CrMoV5-1 steel parts manufactured by casting and evaluation of possible cleavage failure, *Int. J. Metalcasting* 14 (2020) 384–395. [doi:10.1007/s40962-019-00356-7](https://doi.org/10.1007/s40962-019-00356-7)
- [15] A. Pastor, P. Valles, W. More, S. F. Medina, Toughness improvement of steel X38CrMoV5-1 via alternative manufacturing process and prevention of catastrophic failure in safety parts, *Eng. Fail. Anal.* 82 (2017) 791–801. [doi:10.1016/j.engfailanal.2017.07.025](https://doi.org/10.1016/j.engfailanal.2017.07.025)
- [16] A. Pastor, P. Valles, S. F. Medina, Study of phase transformations in steel X38CrMoV5-1 using dilatometry and differential thermal analysis, *Steel Res. Int.* 88 (2017) 1600229. [doi:10.1002/srin.201600229](https://doi.org/10.1002/srin.201600229)
- [17] A. Muehlemann, Interior nucleation of martensite in a cubic-to-tetragonal phase transformation, *Mater. Today: Proceedings* 2S (2015) S605–S609. [doi:10.1016/j.matpr.2015.07.357](https://doi.org/10.1016/j.matpr.2015.07.357)
- [18] V. Leskovsek, B. Sustarsic, G. Jutrisa, The influence of austenitizing and tempering temperature on the hardness and fracture toughness of hot-worked H11 tool steel, *J. Mater. Proc. Technol.* 178 (2006) 328–334. [doi:10.1016/j.jimatprotec.2006.04.016](https://doi.org/10.1016/j.jimatprotec.2006.04.016)
- [19] D. Delagnes, F. Rézad-Aria, C. Levailant, Influence of testing and tempering temperatures on fatigue behaviour, life and crack initiation mechanisms in a 5%Cr martensitic steel, *Procedia Eng.* 2 (2010) 427–439. [doi:10.1016/j.proeng.2010.03.047](https://doi.org/10.1016/j.proeng.2010.03.047)
- [20] G. R. Irwin, *Fracture Dynamics*, In: *Fracturing of Metals*, American Society for Metals, Cleveland, 1948.
- [21] K. Wallin, T. Saario, K. Torronen, Statistical model for carbide induced brittle fracture in steel, *Met. Sci.* 18 (1984) 13–16. [doi:10.1179/030634584790420384](https://doi.org/10.1179/030634584790420384)
- [22] P. Bowen, S. G. Druce, J. F. Knott, Effects of microstructure on cleavage fracture in pressure vessel steel, *Acta Metall.* 34 (1986) 1121–1131. [doi:10.1016/0001-6160\(86\)90222-1](https://doi.org/10.1016/0001-6160(86)90222-1)
- [23] D. A. Curry, J. F. Knott, Effect of microstructure on cleavage fracture toughness of quenched and tempered steels, *Met. Sci.* 13 (1979) 341–345. [doi:10.1179/msc.1979.13.6.341](https://doi.org/10.1179/msc.1979.13.6.341)
- [24] S. Wu, H. Jin, Y. Sun, L. Cao, Critical cleavage fracture stress characterization of A508 nuclear pressure vessel steels, *Int. J. Pres. Vessels Pip.* 123–124 (2014) 92–98. [doi:10.1016/j.ijpvp.2014.08.003](https://doi.org/10.1016/j.ijpvp.2014.08.003)
- [25] D. J. F. Ewing, Calculations on the bending of rigid/plastic notched bars, *J. Mech. Phys. Solids* 16 (1968) 205–213. [doi:10.1016/0022-5096\(68\)90029-X](https://doi.org/10.1016/0022-5096(68)90029-X)
- [26] A. Di Schino, C. Guarnaschelli, Effect of microstructure on cleavage resistance of high-strength quenched and tempered steels, *Mater. Lett.* 63 (2009) 1968–1972. [doi:10.1016/j.matlet.2009.06.032](https://doi.org/10.1016/j.matlet.2009.06.032)
- [27] A. Villuendas, J. Jorba, A. Roca, Change of Young's modulus of hypoeutectoid carbon steels with heat treatment, *Rev. Metal. Madrid, Vol. Extr.* (2005) 46–52. (in Spanish) [doi:10.3989/revmetalm.2005.v41.iExtra.997](https://doi.org/10.3989/revmetalm.2005.v41.iExtra.997)
- [28] P. Brozzo, G. Buzzichelli, A. Mascanzoni, M. Mirabile, Microstructure and cleavage resistance of low-carbon bainitic steels, *Met. Sci.* 11 (1977) 123–130. [doi:10.1179/msc.1977.11.4.123](https://doi.org/10.1179/msc.1977.11.4.123)
- [29] A. Tanaka, S. Tani, C. Ouchi, Low temperature toughness of water-cooled and tempered low carbon manganese steel, *Iron. Steel Inst. Japan* 15 (1975) 19–26. [doi:10.2355/isijinternational1966.15.19](https://doi.org/10.2355/isijinternational1966.15.19)
- [30] Y. Ohmori, H. Ohtani, H. Kunitake, Tempering of the bainite and the bainite/martensite duplex structure in low-carbon low-alloy steel, *Met. Sci.* 8 (1974) 357–366. [doi:10.1179/msc.1974.8.1.357](https://doi.org/10.1179/msc.1974.8.1.357)